International Journal For Technological Research In Engineering
Volume 4, Issue 4, December-2016 *ISSN (Online): 2347 - 4718*

SYNTHESIS OF $La_{1-x}Ca_xMnO_3$ (X=0.5, 0.625) ((ABO3 TYPE MATERIAL) THIN FILM BY PULSE LASER DEPOSITION (PLD) & IT'S CHARACTERIZATION

Kumar Chandan Priydarshi

ABSTRACT: ***Transition -metal perovskite oxides of simple ABO3 perovskite structure can exhibit a wide diversity of functionalities such as the large and tunable ferroelectricity, colossal magnetoresistance, and superconductivity. Furthermore, by stacking different perovskites into epitaxial films, multilayers, and superlattices, the reconstructions of charge, orbital, spin, and lattice degrees of freedom on the nanometer scale may allow not only their properties to be combined but, sometimes, also totally new phenomena to be induced at the heterointerface. Specifically, the reconstructions of the flexible corner-sharing BO6 networks are always intriguing and crucial in perovskite heterostructures. both the experimental and theoretical results have revealed that the epitaxial strain, generated by the lattice constant mismatch at the heterointerface between two dissimilar perovskites, can directly alter the patterns and magnitudes of the octahedral rotation and deformation, then giving rise to structures that are not been found in bulk phase diagram, and even structural transitions as a function of the lattice mismatch, symmetry mismatch, and film thickness. In addition to the strain-mediated elastic octahedral coupling, recently it has been predicted and demonstrated that the corner-connectivity nature of octahedral networks could enable the octahedral rotation/deformation patterns in the substrate to transfer across the interface and imprint into the films, yielding interfacial layers with octahedral configurations unstable in bulk. Unlike the epitaxial strain that can be coherently maintained over tens of nanometers, the interfacial octahedral coupling only persists for several unit-cells. The discovery of colossal magnetoresistance (CMR) effect in divalent alkaline-earth ion doped perovskite manganites ABO3, where A is trivalent rare-earth (La, Pr, Sm, etc.) and B represents divalent alkaline-earth ions (Ca, Sr, Ba), has aroused tremendous interest due to their rich fundamental physics and great potential application in spintronics. Some of the important points of perovskite material are:***

- ***Perovskite structure of ABO3with transition metal ion B gives rise to unique properties like TSC, GMR, and Multiferroic etc.***
- ***It is the d-orbital of B that manifest in magnetic properties.***
- ***Off-centre distortion of B ion gives rise to FE.***

I. INTRODUCTION TO PEROVSKITE STRUCTURE:

The perovskite structure is adopted by many oxides that have the chemical formula ABO3.In the idealized cubic unit cell of such a compound, type 'A' atom sits at cube corner positions (0, 0, 0), type 'B' atom sits at body centre position (1/2, 1/2, 1/2) and oxygen atoms sit at face centred positions (1/2, 1/2, 0). The 'A' atoms are larger than the 'B' atoms. The ideal cubic-symmetry structure has the B cation in 6-fold coordination, surrounded by an octahedron of anions, and the A cation in 12-fold cuboctahedral coordination.[1] Perovskite oxides materials exhibit many interesting and intriguing properties from both the theoretical and from the application point of view. Colossalmagn-etoresistance, ferroelectricity, superconductivity, charge ordering, spin dependent transport, high thermopower and the interplay of structural, magnetic and transport properties are commonly observed features in this family. These compounds are used as sensors and catalyst electrodes in certain types of fuel cells and are candidates for memory devices and spintronics applications. Many superconducting ceramic materials (high temperature superconductors) have perovskite-like structures, often with 3 or more metals including copper, and some oxygen positions left vacant. One prime example is yttrium barium copper oxide which can be insulating or superconducting depending on the oxygen content.

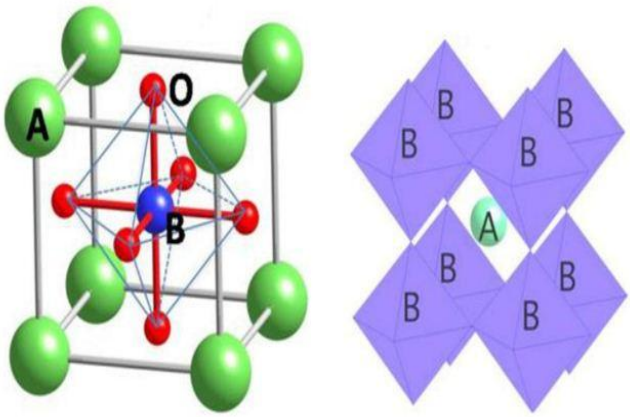

II. DEPOSITION AND CHARACTERIZATION TECHNIQUE

DEPOSITION TECHNIQUE:

The act of applying a thin film to a surface is thin-film deposition any technique for depositing a thin film of material onto a substrate or onto previously deposited layers. "Thin" is a relative term, but most deposition techniques control layer thickness within a few tens of nanometres. Molecular beam epitaxy allows a single layer of atom to be deposited at a time. Deposition techniques fall into two broad categories, depending on whether the process is primarily chemical or physical.

Pulse laser deposition (PLD):

Pulses of focused laser light vaporize the surface of the target

material and convert it to plasma; this plasma usually reverts to a gas before it reaches the substrate. In general, the idea of PLD is simple. A pulsed laser beam is focused onto the surface of a solid target. The strong absorption of the electromagnetic radiation by the solid surface leads to rapid evaporation of the target materials. The evaporated materials consist of highly excited and ionized species. They presented themselves as a glowing plasma plume immediately in front of the target surface if the ablation is carried out in vacuum. Figure 4.1 shows some typical plasma plumes produced during PLD process.

Mechanisms of PLD:
The principle of pulsed laser deposition, in contrast to the simplicity of the system set-up is a very complex physical phenomenon. It involves all the physical processes of laser-material interaction during the impact of the high-power pulsed radiation on a solid target. It also includes the formation of the plasma plume with high energetic species, the subsequent transfer of the ablated material through the plasma plume onto the heated substrate surface and the final film growth process. Thus PLD generally can be divided into the following four stages.

- Laser radiation interaction with the target
- Dynamic of the ablation materials
- Decomposition of the ablation materials onto the substrate
- Nucleation and growth of a thin film on the substrate surface

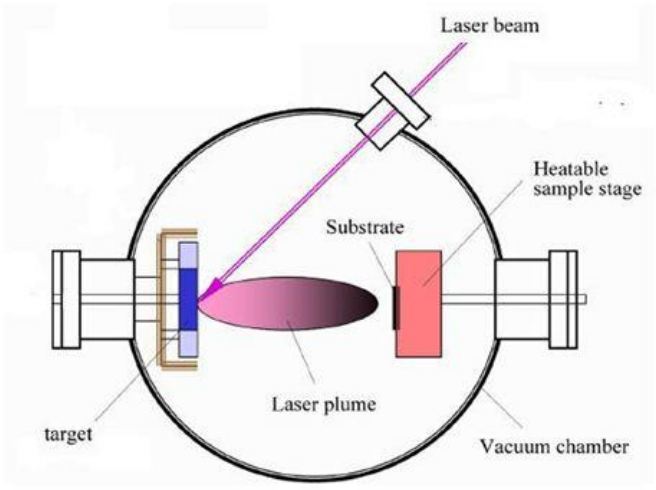

Schematic representation of Pulse Laser Deposition

In the first stage, the laser beam is focused onto the surface of the target. At sufficiently high energy density and short pulse duration, all elements in the target surface are rapidly heated up to their evaporation temperature. Materials are dissociated from the target and ablated out with stoichiometry as in the target. The instantaneous ablation rate is highly dependent on the fluences of the laser irradiating on the target. The ablation mechanisms involve many complex physical phenomena such as collisional, thermal and electronic excitation, exfoliation and hydrodynamics. Nucleation-and-growth of crystalline films depends on many factors such as the density, energy, degree of ionization, and the type of the condensing material, as well as the temperature and the physical-chemical properties of the substrate. The crystalline film growth depends on the surface mobility of the adatom (vapour atoms). Normally, the adatom will diffuse through several atomic distances before sticking to a stable position within the newly formed film. High temperature favours rapid and defect free crystal growth, whereas low temperature or large supersaturation crystal growth may be overwhelmed by energetic particle impingement, resulting in disordered or even amorphous structures.

III. CHARACTERIZATION TECHNIQUE

Composition and Structural Characterization by using XRD technique:
For the structural characterization of 3-D polycrystalline bulk, 2-D thin films of manganites, usually XRD technique is used to identify the phase purity, types of phases and crystallographic structure of the sample. For detailed structural studies like bond length and bond angle variations, magnetic structure refinement etc, ND is a powerful tool. During the course of present work, both the experimental techniques of structural characterization have been used. Three sources of radiation are important: X-rays, synchrotron radiation and neutrons. The laws of diffraction, i.e. the interference of diffracted beams holds equally well for all radiations

X-ray diffraction measurement:
Diffraction occurs when waves interact with a regular structure whose repeat distance is about the same as the wavelength of X-ray waves. X-rays have wavelengths of the order of a few angstroms, the same as typical inter-atomic distances in crystalline solids so they can interact with atoms and can gain the information at atomic level. Crystalline materials can be described by their unit cell which is the smallest unit describing the material. In the material, this unit cell is then repeated over and over in all directions. This will result in planes of atoms at certain intervals. Fig 2.3 shows the schematic representation of x-ray diffractometer.

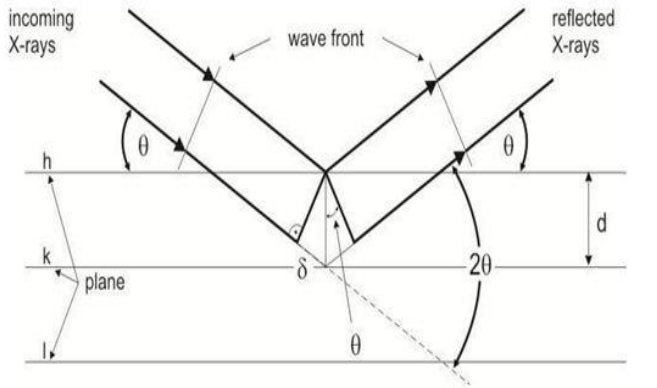

Schematic representation of X-ray diffractometer (Bragg's Law reflection)

X-ray powder diffraction is a powerful non-destructive testing method for determining a range of physical and chemical characteristics of materials. It is widely used in all fields of science and technology. The applications include phase analysis, i.e. the type and quantities of phases present

in the sample, the crystallographic unit cell and crystal structure, crystallographic texture, crystalline size, macro-stress and microstrain, and also electron radial distribution functions. X-ray diffraction results from the interaction between X-rays and electrons of atoms. Depending on the atomic arrangement, interferences between the scattered rays are constructive when the path.

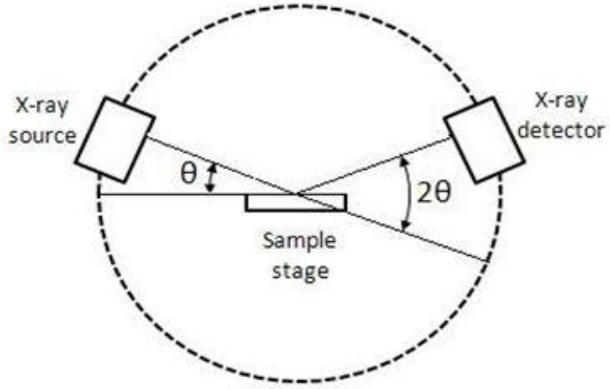

Schematic representation of X-ray diffractometer.

Difference between two diffracted rays differs by an integral number of wavelengths. This selective condition is described by the Bragg equation, also called "Bragg's law":

$$n\lambda = 2\,d\sin\theta$$

Where d = inter planar distance (d-spacing), θ = half angle between incident and reflected beam (or the angle between the incident/reflected beam and particular crystal planes under consideration), n = order of reflection (integer value), λ = wave length of X- rays.

Scherrer equation:

The Scherrer equation, in X-ray diffraction and crystallography, is a formula that relates the size of sub-micrometre particles, or crystallites, in a solid to the broadening of a peak in a diffraction pattern. It is named after Paul Scherrer. It is used in the determination of size of particles. The Scherrer equation can be written as:

$$\tau = \frac{K\lambda}{\beta\cos\theta}$$

Where

- τ is the mean size of the ordered (crystalline) domains, which may be smaller or equalto the grain size;
- K is a dimensionless shape factor, with a value close to unity. The shape factor has atypical value of about 0.94, but varies with the actual shape of the crystallite;
- λ is the X-ray wavelength;
- β is the line broadening at half the maximum intensity (FWHM), after subtracting the instrumental line broadening, in radians. This quantity is also sometimes denoted as
- Δ(2θ);
- θ is the Bragg angle.

IV. EXPERIMENTAL WORK AND RESULT DISCUSSION

SYNTHESIS AND EXPERIMENTAL DETAILS:

The bulk polycrystalline sample of $La_{1-x}Ca_xMnO_3$ (LCMO) with X= 0.5, 0.625 was synthesized using conventional solid state reaction route (SSR). Various steps involved in the synthesis of bulk LCMO samples are shown in fig 3.1. The high purity starting materials, La_2O_3, $CaCO_3$ and MnO were mixed in stoichiometric ratios and calcined at 900°C for 24 hours. The calcined powder was then grounded, pelletized and sintered at various temperatures between 900 - 1150°C with intermediate grindings before final sintering at 1150°C.

$La_{1-x}Ca_xMnO_3$ (X=0.5, 0.625) weight calculation:

Compound	$La_{0.5}Ca_{0.5}MnO_3$	Wt %	Stoichiometry ratio	Req wt.	3.5
La_2O_3	325.8091	0.25	81.452275	0.402366337	1.40828218
$CaCO_3$	100.0869	0.5	50.04345	0.247209788	0.865234259
MnO	70.9374	1	70.9374	0.350423875	1.226483561
			202.433125	1	3.5
	$La_{0.375}Ca_{0.625}MnO_3$				3.5
La_2O_3	325.8091	0.1875	61.08920625	0.313952707	1.098834476
$CaCO_3$	100.0869	0.625	62.5543125	0.321482255	1.125187892
MnO	70.9374	1	70.9374	0.364565038	1.275977632
			194.5809188	1	3.5

Weight calculation

After that this pellet was used for deposition process. Different LaAlO3 (LAO) (100), (LaAlO3)0.3 (Sr2AlTaO6)0.7 (LSAT) (100) substrates were used for deposition by this bulk material by using Pulse laser deposition.

V. FLOW CHART

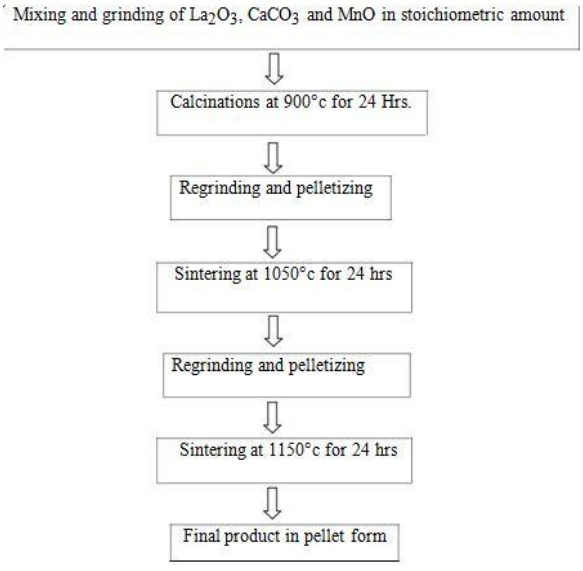

Fig 3.1: Flow chart of synthesis of magnetite $La_{1-x}Ca_xMnO_3$

(X=0.5, 0.625) (LCMO) through SSR method
Process Parameter:
Source material (pellets)→ $La_{1-x}Ca_xMnO_3$ (X=0.5)/ LAO substrate (100) and $La_{1-x}Ca_xMnO_3$ (X=0.625)/ LSAT substrate (100)
Temperature(c) →710°C
Frequency (Hz)→ 4Hz
Energy mJ→ 300mJ
Annealing pressure → 1000 Pa

VI. RESULT AND DISCUSSION

XRD Spectrum analysis:
XRD spectra are measured by using Cu-Kα radiation in panalytical X-ray diffractomer. Following is the XRD pattern of polycrystalline bulk sample. Fig 3.2 and Fig 3.3 shows the Phase purity of bulk material devoid of any extra peaks in its XRD pattern and the polycrystalline structure of the material.
XRD Spectrum of $La_{0.5}$ $Ca_{0.5}$ MnO_3 polycrystalline samples:

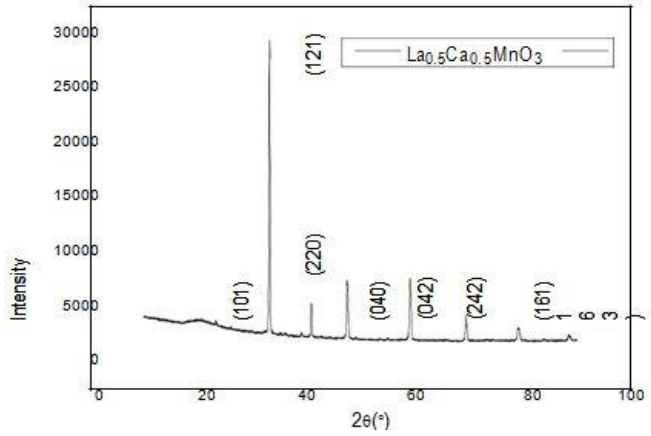

X-ray diffraction pattern of $La_{0.5}Ca_{0.5}MnO_3$ polycrystalline samples

Major peaks were observed at 2-theta values (22.98) (33.18) (40.99) (47.50) (59.01) (69.84) (79.39) and (88.93) which match the peaks reported in literature [7] corresponding to the (101) (121) (220) (040) (042) (242) (161) and (163) planes and full width half maxima (FWHM) at major peak is 0.19055(degree) at 2- theta 33.18 in Fig 3.2, and its size of particle of major peak is 45.46 nm.
XRD Spectrum of La0.5 Ca0.5 MnO3 polycrystalline samples:

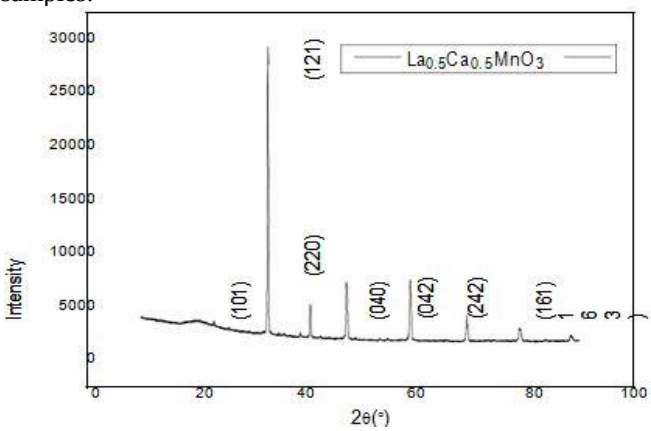

X-ray diffraction pattern of $La_{0.5}Ca_{0.5}MnO_3$ polycrystalline samples

Major peaks were observed at 2-theta values (22.98) (33.18) (40.99) (47.50) (59.01) (69.84) (79.39) and (88.93) which match the peaks reported in literature [7] corresponding to the (101) (121) (220) (040) (042) (242) (161) and (163) planes and full width half maxima (FWHM) at major peak is 0.19055(degree) at 2- theta 33.18 in Fig 3.2, and its size of particle of major peak is 45.46 nm.

XRD Spectrum of $La_{0.375}$ $Ca_{0.625}$ MnO_3 Polycrystalline Samples:

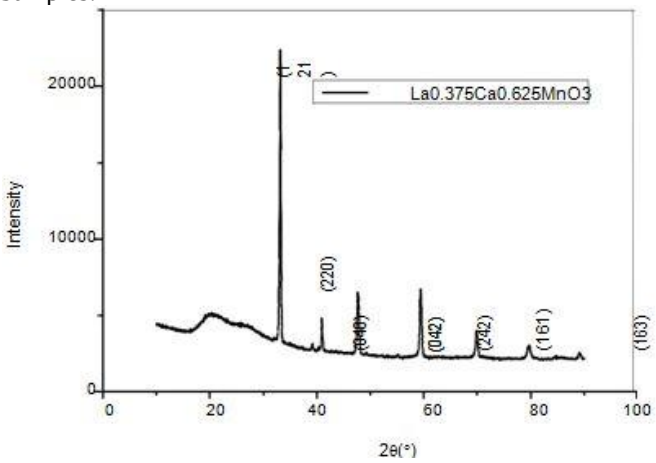

X-ray diffraction pattern of $La_{0.375}Ca_{0.625}MnO_3$ polycrystalline samples

Major peaks were observed at theta values (33.409) (40.1) (47.7) (59.44) (69.84) (79.60) and (88.93) which match the peaks reported in literature [7] corresponding to the (121) (220) (040) (042) (242) (161) and (163) planes and full width half maxima (FWHM) at major peak is 0.2951404(degree) at 2- theta 33.1347 in Fig 3.3, and its size of particle of major peak is 29.34nm in Fig 3.3.

XRD Spectrum of thin film $La_{0.5}Ca_{0.5}MnO^3$ /LAO (100):

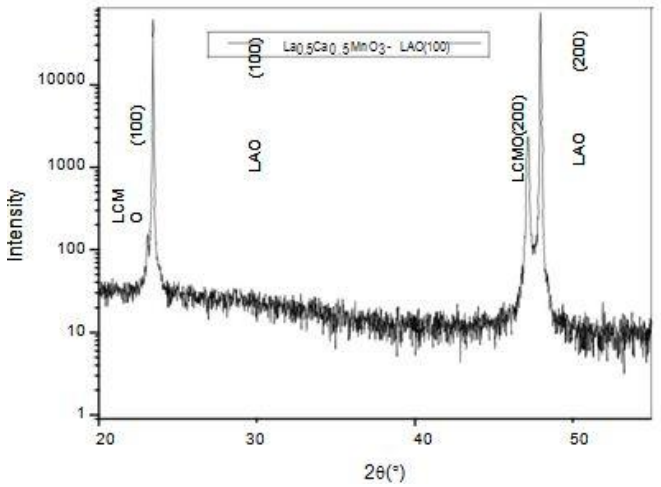

Fig 3.4 X-ray diffraction pattern of $La_{0.5}Ca_{0.5}MnO_3$ /LAO (100) thin film

Fig 3.4 shows the θ-2θ scan of compressive strained $La_{0.5}Ca_{0.5}MnO_3$ film grown on LAO (100) oriented substrate. XRD pattern confirms the phase purity and epitaxial nature of the $La_{0.5}Ca_{0.5}MnO_3$ thin film grown on the LAO (100) substrate with absence of any impurity peaks.[4]

REFERENCES

[1]. Robert S. Roth(Journal of Research of the National Bureau of Standards Vol. 58, No.2, (February 1957).
[2]. Wenbin Wu, K. H. Wong, X.-G. Li, and C. L. Choy, Y. H. Zhang Appl. Phys. Vol. 87, No. 6, (15 March 2000)
[3]. C. J. Lu, Z. L. Wang, C. Kwon, and Q. X. Jia, Appl. Phys Vol. 88, No 7,(Oct 2000)
[4]. M. Ziese, H. C. Semmelhack, K. H. Han, S. P. Sena, and H. J. Blythe J. Appl. Phys., Vol. 91, No. 12, (15 June 2002)
[5]. Yu. A. Boikov, R. Gunnarsson, and T. Claeson; J. Appl. Phys., Vol. 96, No. 1, (1 July

